Journal: Journal of Constructional Steel Research

Title: MODELING COMPOSITE BEAMS WITH PARTIAL INTERACTION

ID: JCSR-D-15-00095

Authors: Turmo, J., Lozano-Galant, J.A., Mirambell, E. and XU, D.

1- Introduction

In the last decades, the use of concrete and steel composite beam structural systems has received significant attention both numerically (e.g. Martinelli et al. (2012), Zona and Ranzi (2014), Huang et al. (2014), Danku et al. (2013a)) and experimentally (e.g. Al-deen et al. (2011), Soty and Shima (2013), Guezouli, S. Lachal (2012), Hsu et al. (2014), Danku et al. (2013b) and Kim et al (2014)). This popularity is due to their construction speed together with structural and cost advantages. In a steel-concrete composite beam the tensile strength of the steel and the compressive strength and mass of the concrete slab are exploited. These two materials are connected with shear struts so that they act compositely. For a composite beam with rigid shear connection, there is full interaction between the steel and the concrete members. In this case, there is no relative slip at the interface of both materials and Navier hypothesis is fully applicable. This approach is followed by most codes (e.g. the rigid-ideal plastic method in Eurocode 4 (1994a) and (1994b)). Nevertheless, all shear connections are flexible to some extent and therefore, full interaction is rarely achieved in practice. For this reason, partial interaction (see e.g. Wang and Chung (2006), Nie et al. (2008), Razi and Bradford (2009) and Degtyarev (2014)), with a relative slip at the interface, commonly appears in actual structures. The simulation of this relative slip is of primary importance because it affects both the deflections and the stresses in both the concrete and steel members. Therefore, partial interaction occurs to some extent in all beams weather fully connected or not. However, according to Queiroz et al. (2007), any flexibility in the connection may be ignored for beams designed for full connection.

A number of studies has been carried out to simulate the behavior of composite beams with partial shear interaction. According to many authors (see e.g. Sousa et al. (2010)), the first analytical model including partial shear interaction for beams is attributed to Newmark et al. (1951). In this method, the equilibrium and compatibility equations for an element of the composite beam are reduced to second order differential equations. This model assumes distributed bonds at the concrete-steel interface. These bounds enforce contact between components and allow longitudinal interlayer slip. The differential equation approach of this method was also followed by Martínez and Ortiz (1975), who defined the analytical solutions for elastic simply supported composite beams under simple loading cases. This procedure assumes that the deflections of the centroids of steel and concrete cross-sections are the same and continuous connection at the concrete-steel interface. The main inconveniences of these analytical methods are as follows: (1) Obtaining the analytical equation of any simple load case requires many efforts. (2) The analysis is complex and costly to apply and is limited to some particular load cases and their combinations. (3) The effects of the actual non-continuous shear struts cannot be studied. For all these reasons, the analytical approach is far from being suitable for practical design [Turmo and Mirambell (1999)]. Alternatively, numerical methods have propitiated the development of approximated analysis procedures that are more suitable for practical design than analytical equations. Examples of approximated methods can be found in the literature (see e.g. Proco et al. (1994), Szabó (2006), Park et al. (2013), Sakr and Sakla (2009)). Among these procedures, it is to highlight the finite element model simulation. This issue has received considerable attention in the last years.

A major concern of the simulation of composite beams by Finite Element Model (FEM) analysis lays on the model dimensionality. Many researches (such as Daniels and Crisinel (1993), Salari et al. (1998) or Dall'asta and Zona (2002)) have proved that one-dimensional finite element models can be used to simulate satisfactorily the global behavior of composite beams. Nevertheless, these are not adequate to simulate the local responses, such as the distribution of stresses in concrete and steel components and in their interface. This limitation made research focus on 2D and 3D models to simulate the behavior of composite beams (see e.g. Mizra and Uy (2010)). On the one hand, 3D models are especially adequate for accurate simulation of local aspects of composite structures. An example of their application is to define an accurate distribution of stresses at discontinuity sections. Nevertheless, according to Queiroz et al. (2009) the numerical convergence problem and the large computation times of these models discourage its use for complex structural systems. Although the recent development of adequate software, such as ABAQUS/ explicit (see e.g. Prakash et al. 2011 or Tahmasebinia et al. 2013), has improve considerably the convergence, and therefore, the applicability of the 3D models, many authors agree that 2D models might still be preferred for practical design work. A detailed review of some of the main 2D and 3D models presented since the eighties is presented by Titoum et al. (2008). Many authors (see e.g. Queiroz et all 2007), have presented shell element models using springs to simulate the behavior of the connection. These models might be very accurate. In fact, they are able to simulate local effects, such as the crippling of thin walled sections (e.g. I beam web) including shear deformation. Nevertheless, the accuracy of the shell element models is associated with two problems: (1) The results of these models cannot be directly used in design, as integration of stresses is required. (2) Especially in large scale structures, shell element models might result more computationally challenging than beam element models. Because of these problems, beam element models might be preferred as they provide relatively accurate results to be used in design with lower computational effort. Furthermore, shear deformation can be included. One of the methods based on 2D simulation by linear frame elements is presented in Queiroz et al. (2009.a and b). In this method, the concrete-steel interface is simulated by discrete nonlinear springs located at the concrete centroid.

This paper aims to provide a structured approach to the simulation of the partial interaction behavior using simple finite element software. To do so, a model uniquely composed of beam elements is proposed. This model directly provides useful information for the design work without the need of stress integration. To do so, it proposes a two-dimensional finite element model to analyze the behavior of composite beams with partial interaction and arbitrary boundary and loading conditions. In this model, the different elements of the composite beams are modeled by six different types of frame elements (concrete slab, steel beam, vertical struts, spring shear connector elements and elements representing concrete thickness and steel thickness). Compared with the analytical equations presented in the literature, the main advantages of the proposed model are as follows: (1) Intuitiveness, as each of the elements of the model presents a close and easy to understand relation with the structural behavior of composite beams. (2) Applicability, as the method directly provides useful information (such as forces in steel beam and concrete slab, shear connector forces or beam deflections) for the design work. (3) Versatility and generalization in dealing with any combination of loading and boundary conditions. The proposed model enables the analysis of statically indeterminate structures, tapered beams, frames as well as structures with non-uniform shear connector distributions. Furthermore, this model might be easily modified to deal with 3D structures and nonlinear behavior of concrete slab, steel beam and shear connectors. (4) As the models include sequences of repetitive elements, they can be easily elaborated by simple preprocessing algorithms. (5) As the model only includes frame elements, the model behavior can be easily reproduced by simple structural software.

The paper is organized as follows: In Section 2, the analytical equations presented in the literature to define the behavior of simply supported composite beams under different loading cases are reviewed. In Section 3, the main characteristics of each of the elements of the proposed frame model are described in detail. In Section 4, the numerical application of the model to two different examples (a simply supported and a continuous composite beam) is presented. To validate the accuracy and the efficiency of the proposed model, this section includes different FEMs verified against the results of the analytical equations. In this analysis, the effects of the connection stiffness and the geometrical and mechanical properties of the beam elements are also studied. Finally, some conclusions are drawn in Section 5.

2- Composite beams with partial shear interaction: Analytical approach

The analytical equations of composite constant depth simply supported beams with partial interaction under simple load cases can be found in Martínez and Ortiz (1975) (Equations (1)-(4)). In this procedure, the equilibrium equations of the composite beam are reduced to second order differential equations from which analytical results can be obtained. These equations are based on the following assumptions: (1) The shear connectors, as well as concrete and steel, behave linearly. (2) Concrete slab and steel beam have the same curvature (and same rotation) throughout the length of the composite beam. (3) Frictional effects and uplift at the concrete-steel interface are neglected. (4) The discrete shear connectors at the concrete-steel interface are uniform throughout the length composite beam. With k_q being the connector stiffness under shear force, s_q being the shear connector longitudinal spacing and n_q being the number of shear struts in every row separated s_q, the distributed constant stiffness of the shear connections throughout the beam is assumed as $K_q=(n_q \cdot k_q)/s_q$. These parameters are illustrated in Figure 1.A.

As an example of the results of the analytical approach, the analytical equations for concrete slab axial forces at cross section *x*, $N_c(x)$, for different loading cases are presented as follows:

$$N_{c,Q}(x) = \frac{-M(x)}{a_{cr}} \cdot \psi_Q = \frac{-M(x)}{a_{cr}} \cdot \left(1 - \frac{ch\left(\frac{l}{2 \cdot x_q}\right) - ch\left(\frac{l}{2 \cdot x_q} - \frac{x}{x_q}\right)}{\frac{x}{x_q} \cdot \frac{(l-x)}{x_q} \cdot ch\left(\frac{l}{2 \cdot x_q}\right)} \right) \quad (1)$$

$$N_{c,q}(x) = \frac{-M(x)}{a_{cr}} \cdot \psi_q = \frac{-M(x)}{a_{cr}} \cdot \left(1 - \frac{x}{x_q} \cdot \frac{sh\left(\frac{x}{x_q}\right)}{ch\left(\frac{l}{x_q}\right)} \right) \quad (2)$$

$$N_{c,M}(x) = \frac{-Mext \cdot x}{L \cdot a_{cr}} \cdot \psi_M = \frac{-Mext \cdot x}{L \cdot a_{cr}} \cdot \left(1 - \frac{sh\left(\frac{x}{x_q}\right)}{\frac{x}{l} \cdot sh\left(\frac{l}{x_q}\right)} \right) \quad (3)$$

$$N_{c,P}(x) = -\zeta_C \cdot P - \zeta_S \cdot P \cdot \xi_S = -\left(1 + \frac{A_s^2 \cdot h_{sc}^2}{A_R \cdot I_R}\right) \cdot \frac{A_{cR} \cdot P}{A_R} - \left(1 - \left(1 + \frac{A_s^2 \cdot h_{sc}^2}{A_R \cdot I_R}\right) \cdot \frac{A_{cR}}{A_R}\right) \cdot P \cdot \frac{ch\left(\frac{x}{x_q} - \frac{l}{2 \cdot x_q}\right)}{ch\left(\frac{l}{2 \cdot x_q}\right)} \quad (4)$$

in which $N_{C,Q}(x)$ is the axial force when a concentrated load *Q* is applied at mid-span, $N_{C,q}(x)$, is the axial force when a constant distributed vertical load *q* is applied throughout the beam, $N_{C,M}(x)$, is the axial force when a concentrated external bending moment, M_{ext}, is applied at one beam edge, and $N_{C,P}(x)$, is the axial force when a concentrated prestressing load P is introduced at both beam edges and applied at the centroid of the concrete slab. In these equations $M(x)$ is the bending moment at cross section *x*, E_c and E_s are the Young's modulus in concrete slab and steel beam, A_R and I_R are the area and the inertia of the reduced composite section, A_{cR} and I_{cR} are the reduced area and inertia of the concrete section, A_S and I_S are the area and inertia of the steel section, h_{sc} is the distance between the concrete slab and the steel beam centroids, a_{cR} and x_q are coefficients defined as presented in Equations (5) and (6).

$$a_{cR} = \frac{I_R \cdot A_R}{h_{sc} \cdot A_{cR} \cdot A_S} \quad (5)$$

$$x_q = \sqrt{\frac{(I_S + I_{cR}) \cdot s_q \cdot E_S}{a_{cR} \cdot h_{sc} \cdot n_q \cdot k_q}} \quad (6)$$

The first term of Equations (1), (2) and (3) represents the axial force of the concrete partial cross section in composite beams with full interaction between steel beam and concrete slab. On the other hand, the second term of these equations (ψ_Q, ψ_q and ψ_M, respectively) includes the effect of the deformability of the shear connection at the concrete-steel interface. In the case of the prestressing load (in Equation (4)) the axial force for full interaction corresponds to the term $\zeta_C \cdot P$, while $\zeta_S \cdot P \cdot \xi_S$ includes the effects of the partial interaction.

In addition to their computational cost, the limitation of the analytical equations refers to their application restrictions. In fact, these equations cannot be applied in a number of practical design solutions (such as tapered beams, non-continuous shear connector distributions or complex load cases). For continuous beams, support reactions are unknown. For this reason, these structures cannot be analyzed with those formulae unless it is assumed that the reactions of a continuous beam are not affected by the partial interaction.

3- Description of the proposed model.

The model presented to study the structural behavior of composite beams with partial interaction (as the one presented in Figure 1.A) is based on an intuitive elastic and linear FEM. In this model, six different types of beam elements are used to achieve the first three assumptions followed in the analytical equations described in the preceding section. The six frame elements of the proposed model are as follows:

1. Elements type 1 for concrete slab: These beam elements model the concrete slab. Therefore, these elements include the same properties of the concrete slab at its centroid (presented in Figure 1.A).
2. Elements type 2 for steel beam: These beam elements model the steel beam and they include the same properties of the steel beam at its centroid (presented in Figure 1.A).
3. Elements type 3 for vertical struts: These truss elements connect vertically the nodes of the concrete and the steel beams (nodes of elements type 1 and 2). The element type 3 has no weight, infinity area and null inertia and might be uniformly spaced a length *V*. This element equals the vertical deflections at the centroids of steel and concrete sections throughout the beam length. This condition can be mathematically expressed as follows:

   $$\frac{M_c(x)}{E_c \cdot I_c} = \frac{M_s(x)}{E_s \cdot I_s} \quad (7)$$

   in which, $M_c(x)$ and $M_s(x)$ are the bending moments along the x axis of concrete and steel sections, respectively.
4. Elements type 4 for shear connector springs. These elements simulate the effects of the stiffness k_q of the shear connectors illustrated in Figure 1.A. These elements correspond with axial linear springs located at the concrete-steel interface. The shear connector springs have no bending stiffness. With *S* being the spring spacing, s_q being the shear connector longitudinal spacing, L_4, being the arbitrary length of element type 4, A_4 being the arbitrary area of element type 4, the Young's modulus of element type 4, E_4, can be defined assuming that the axial rigidity of the element is equal to the shear connection stiffness as presented in the following equation:

   $$E_4 = \frac{n_q \cdot k_q \cdot L_4 \cdot S}{A_4 \cdot s_q} \quad (8)$$

5. Elements type 5: These beam elements simulate the distance between the concrete centroid and the steel-concrete interface of the composite beam (see Figure 1.A). These elements connect the concrete nodes with the shear connectors at the concrete-steel interface (nodes of element types 1 and 4). These elements have infinity axial and flexural stiffnesses. If the shear connectors are uniformly distributed these elements might be spaced a length *S* throughout the beam. With h_c being the concrete thickness, u_c being the horizontal displacement at the concrete beam node and θ_C its rotation they enable the following horizontal movement u_c^1 at the concrete-steel interface for rectangular sections:

$$u_c^1 = u_c \ - \frac{\theta_c \cdot h_c}{2} \tag{9}$$

6. Elements type 6. These frame elements simulate the distance between the steel centroid and the steel-concrete interface of the composite beam (see Figure 1.A). These elements connect the steel nodes with the shear connectors at the concrete-steel interface (nodes of element types 2 and 4). These elements include infinity axial and flexural stiffnesses. If the shear connectors are uniformly distributed these elements might be spaced a length *S* throughout the beam. With h_s being the height of the steel beam, u_s being the horizontal displacement at the steel beam node and θ_s its rotation they enable the following horizontal movement u_s^1 at the concrete-steel interface for a y-symmetric cross section beam:

$$u_s^1 = u_s \ + \frac{\theta_s \cdot h_s}{2} \tag{10}$$

The boundary conditions of the FEM are located at the steel beam centroid. This is appreciable in Figure 1.B, where a possible FEM to simulate the composite beam in Figure 1.A is presented. This figure also illustrates the six different element types described above and their location.

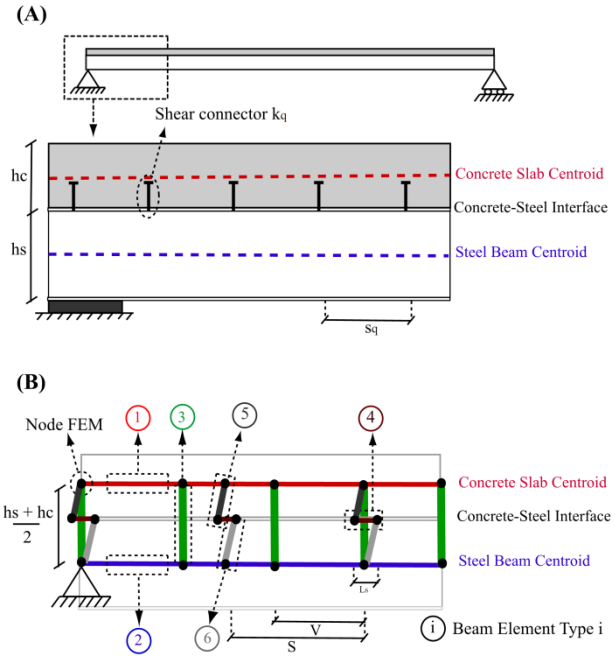

Figure 1: (A) Composite Beam, (B) Proposed model to simulate the structural behavior of the composite beam.

The main characteristics of each of the element types of the proposed FEM are summarized in Table 1. In this table the infinity symbol, ∞, is used to indicate that the corresponding value is very high.

Table 1: Characteristics of the different elements of the proposed *FEM*. (*E*=Young's Modulus, *A*=Area, *I*=Inertia).

Element type	*E*	*A*	*I*
1 (Concrete beam)	E_C	A_C	I_C
2 (Steel beam)	E_S	A_S	I_S
3 (Vertical strut)	$E \approx \infty$	$A \approx \infty$	0
4 (Connector spring)	E_4 (Eq. (8))	A_4	0
5 (Concrete thickness)	$E \approx \infty$	$A \approx \infty$	$I \approx \infty$
6 (Steel depth)	$E \approx \infty$	$A \approx \infty$	$I \approx \infty$

The analysis by means of any simple structural software of the proposed FEM provides information useful for design. The obtained results might be summarized as follows: (1) Beam deflections throughout the composite beam axis. (2) Relative slip between the concrete slab and the steel beam. (3) Axial forces and bending moments at the centroids of the concrete slab and the steel beam. This has the advantage that these efforts can be used directly for design, without no need of integrating stresses. (4) Axial forces at the spring connectors. These forces are strongly related with the shear per unit length throughout the steel-concrete interface. (5) Reactions at the boundary conditions.

4-Application of the proposed method

In this section the numerical application of the model proposed in Section 3 is presented. In this application, two composite beams are analyzed. The first structure (Example 1) corresponds with a simply supported composite beam, while the second one (Example 2) corresponds with a three-span continuous composite beam.

4.1- Example 1: Simply supported composite beam

In this section a simply supported composite beam is analyzed. After describing the main characteristics of the structure, three parametric analyses are carried out. In order to study the sensitivity of the composite behavior, the first of these analyses studies the effect of the size of the FEMs. To do so, the results obtained by the analytical equations of Martínez and Ortiz (1975) are compared with those obtained by different FEMs including changes in the separation of vertical struts (number of elements type 3) and shear connector springs (number of elements type 4, and hence 5 and 6). The second parametric analysis illustrates the effect of the stiffness of the concrete and steel connection, K_q. Finally, the third parametric analysis shows the effects of the depth of the steel beam. This study includes a comparison between the results obtained by the analytical equations and those obtained by *FEMs* with different I beams.

4.1.1- Description of the structure

The first analyzed example corresponds with the 4.5m length simply supported composite beam presented in Figure 2.A. This structure includes a 1m width and h_c=0.2m thick concrete slab that is connected with an IPE300 (with a depth, h_S, of 0.3m). The Young's modulus of concrete, E_c, and steel, E_S,

are 3.2E7 kN/m^2 and 2.1E8 kN/m^2, respectively. The connection between both materials is carried out by mean of two shear connectors spaced every 30cm. The stiffness of each shear connector, k_q, is 170000 kN/m. In this way, the stiffness of the connection K_q is 1.13E6kN/m^2.

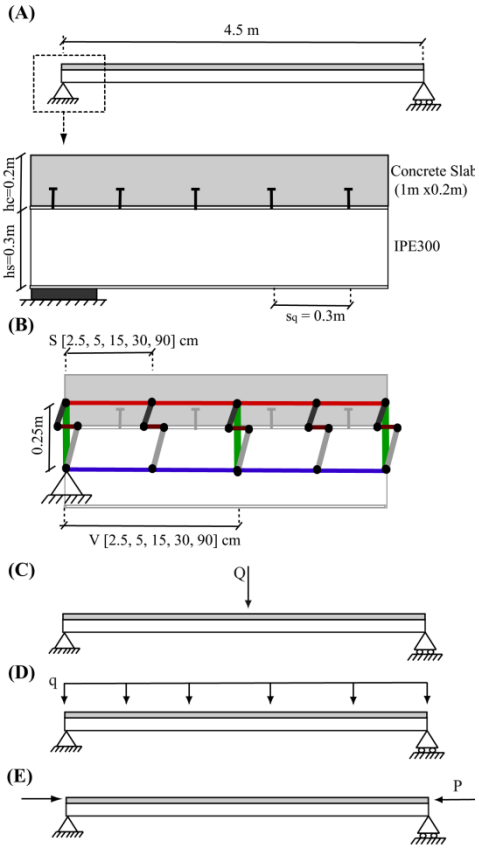

Figure 2: Example 1: (A) Geometry, (B) Studied Models, (C) Concentrated load Q, (D) Uniform load, q, and (E) Prestressing load, P.

The structural behavior of the composite beam is analyzed by a set of different FEMs. Differences between these models refer to: (1) Different spacing among spring elements, *S*, formed by elements type 4, 5 and 6. The studied spacing between spring connectors might be either uniform or non-uniform depending on the distribution of the actual shear connectors. Only uniformly spaced spring connectors are considered in this analysis. The spacing used is 2.5, 5, 15, 30 and 90cm. These distributions are named $S_{2.5}$, S_5, S_{15}, S_{30} and S_{90}, respectively. (2) Different spacing among Vertical struts, *V*, that is to say elements type 3. As in the case of the spring connectors, the studied spacing is 2.5, 5, 15, 30 and 90cm. These distributions of struts are called $V_{2.5}$, V_5, V_{15}, V_{30} and V_{90}, respectively. The combination of the different Spring connectors and Vertical struts distributions leads to a number of 25 different FEMs presented in Figure 2.B. Every FEM is named by their spacing (e.g. S_5V_{30} is a model with Spring connectors every 5cm and Vertical struts every 30cm). The main characteristics (Young's modulus, *E*, Area, *A*, and Inertia, *I*) of each of the elements of the different FEMs are listed in Table 2. All the FEMs (referred in table as $S_{2.5\ to\ 90}V_{2.5\ to\ 90}$) share the characteristics of the first five element types. Nevertheless, this is not the case of the spring connector element which depend to a great extent on the spring spacing, obviously the higher the spacing the higher the axial stiffness of the springs. The Young's modulus for each spring spacing is calculated by Equation (8) assuming an arbitrary spring area, A_4, of 1E-3m^2 and an

arbitrary spring length, L_4, of 0.075m. Note that the Young's modulus of the edge springs is half of that presented in Table 2 because their tributary lengths are half of that of the inner shear connector springs.

Table 2: Characteristics different elements of the FEMs.

Element type	FEMs	E (kN/m^2)	A (m^2)	I (m^4)
(1) Concrete slab	$S_{2.5\ to\ 90}V_{2.5\ to\ 90}$	3.20E7	2.00E-1	6.67E-4
(2) Steel beam	$S_{2.5\ to\ 90}V_{2.5\ to\ 90}$	2.1E8	5.38E-3	8.36E-5
(3) Vertical struts	$S_{2.5\ to\ 90}V_{2.5\ to\ 90}$	1.00E10	1.00E10	0
(4) Connector spring	$S_{2.5}V_{2.5\ to\ 90}$	4.25E5	1.00E-3	0
	$S_5V_{2.5\ to\ 90}$	8.50E5	1.00E-3	0
	$S_{15}V_{2.5\ to\ 90}$	2.55E6	1.00E-3	0
	$S_{30}V_{2.5\ to\ 90}$	5.10E6	1.00E-3	0
	$S_{90}V_{2.5\ to\ 90}$	1.53E7	1.00E-3	0
(5) Concrete thickness	$S_{2.5\ to\ 90}V_{2.5\ to\ 90}$	1.00E10	1.00E10	1.00E10
(6) Steel depth	$S_{2.5\ to\ 90}V_{2.5\ to\ 90}$	1.00E10	1.00E10	1.00E10

In order to ease the comparison with the analytical equations, the effects of three simple load cases have been studied. These load cases are as follows: (1) Concentrated load, Q_m, of 100kN at the mid span of the concrete slab, m. (2) Constant distributed load, q, of 10kN/m on the concrete slab. (3) Two concentrated axial loads (prestressing), P, of 100kN applied at the centroids of the edges of the concrete slab. Each of these load cases are presented in Figure 2.C, 2.D and 2.E, respectively.

It is clear to notice that in small structures, placing a spring element at the location of the actual connector might not be a computational issue. Nevertheless, this might not be the case in large scale structures where a minimization of the number of elements in the model (without a reasonable lack of accuracy) might be required. Obviously, the spacing of the spring connectors and vertical struts plays an important role in the number of both nodes and beam elements in the FEMs. This is appreciable in Figures 3.A and 3.B where the minimum number of nodes and beam elements of each FEM are presented. It is important to highlight that in these figures each model (S_iV_j) is represented by the intersection of the corresponding spacing S_i and V_j. The analysis of Figure 3.A shows that the number of nodes of the FEMs ranges from 540 ($S_{2.5}V_{2.5\ to\ 90}$) to 15 ($S_{90}V_{90}$). In the case of the beam elements, they range from 1080 ($S_{2.5}V_{2.5}$) to 30 ($S_{90}V_{90}$).

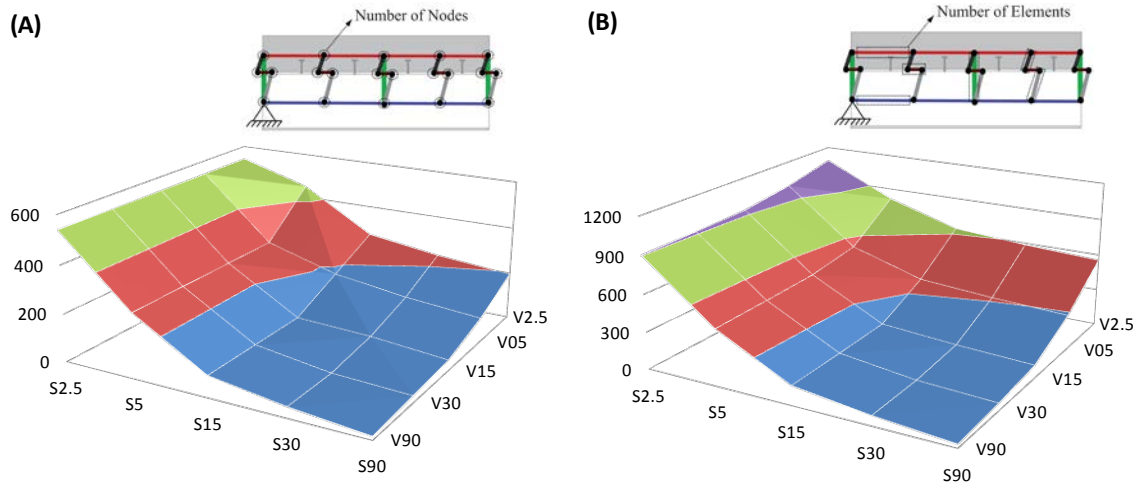

Figure 3: Characteristics of the FEMs of Example 1: (A) Number of nodes and (B) Number of elements. The result of each FEM (S_iV_j) is obtained by the intersection of the spacing S_i and V_j.

4.1.2 Comparison with the analytical equations

In this section, a parametric analysis is presented to illustrate how the spring connector and vertical strut spacing influence the behavior of the FEMs. To do so, the results of the Analytical Equations, *AE*, presented in Martínez and Ortiz (1975) are compared with those obtained by the FEMs described in the preceding section. This comparison is based on two parameters: (1) Beam deflection, f_m, at mid span, m. (2) The axial force at the centroid of the concrete slab, N_{cm}, at mid span, *m.*

The percentage differences between the results obtained by the FEMs and the *analytical equations* are calculated as follows:

$$\left|\frac{N_{cm}(S_iV_j) - N_{cm}(AE)}{N_{cm}(AE)}\right| \tag{11}$$

$$\left|\frac{f_m(S_iV_j) - f_m(AE)}{f_m(AE)}\right| \tag{12}$$

The differences obtained by Equations (11) and (12) for load cases *Q* and *q* are summarized in Figure 4. This figure also illustrates the parameters N_{cm} and f_m. Differences in the load case *P* (prestressing) are not included in this figure because they were negligible.

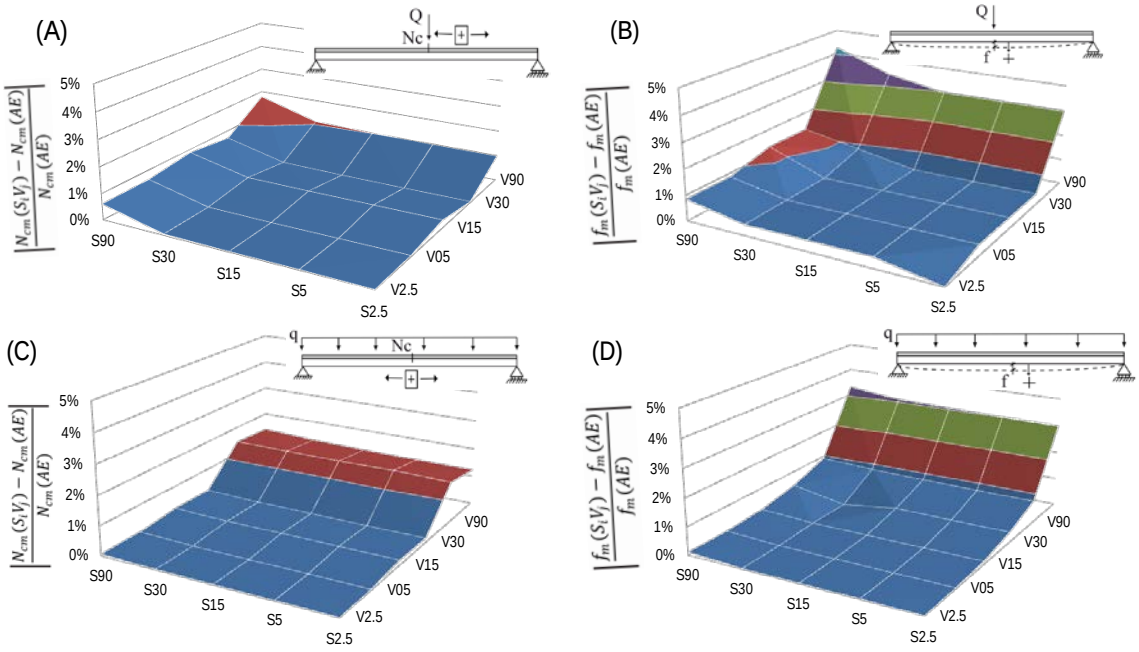

Figure 4: Comparison of the results of different FEMs with the Analytical Equations, *AE*: (A) N_{cm} for *Q*, (B) f_m for Q, (C) N_{cm} for *q* and (D) f_m for q. The result of each FEM is obtained by the intersection of the spacing S_i and V_j.

The differences in Figure 4 might be not only related with the way (location and shape) the load is applied, but also with the model geometry (location of the Vertical struts, V, and the Springs, S, elements). In fact, this figure shows that the higher differences appear in model $S_{90}V_{90}$ when the concentrated load at mid span is applied. It is to notice that, as this model includes neither vertical strut nor spring elements at the beam mid span, the load is directly applied to an inner point of a concrete element (element type 1). The difference of this model with the analytical equations might be explained by the local bending produced in the concrete element. Obviously, this effect is avoided when the concentrated load is directly applied to a node including either a vertical strut or a spring element (that is to say, in models with lower V and S spacing). Obviously, the higher the spacing between vertical struts and spring connectors, the higher the

differences. This is appreciable by the fact that the maximum differences are found in model $S_{90}V_{90}$. For this model, the maximum differences of N_{cm} and f_m are 1.76 and 4.26% for Q and 1.38 and 3.30% for q. The results presented in Figure 4 also illustrate that increasing the spacing of the spring connectors in the FEM increases the differences with the analytical equations more than increasing the spacing of the vertical struts (or in other words, the role of the spring connector spacing is more important than the role of the vertical strut spacing).

The values of N_{cm} obtained by the FEMs were lower than those obtained by the analytical equations. In fact, the lower the number of elements in the FEM the lower the obtained N_{cm} and the higher the differences with result of the Analytical Equations, *AE*. In the case of f_m, the FEMs present higher values than the *AE*. The signs of these differences are explained by the fact that the *AE* assumes a continuous stiffness at the steel-concrete interface. This continuous interface produces higher stiffness than the actual one (with discrete shear connection). This higher stiffness results in higher values of N_{cm} and lower values of f_m when the results of the *AE* are compared with those of the FEMs.

Note that the analytical solution might be regarded as the exact solution. This is misleading, as the physical behavior of the discrete behavior of the shear connectors might be best modeled by the FEM. This is achieved introducing the spring elements there where the shear connectors are presented (S_{30}). Even though the most accurate simulation of the physical behavior is achieved when a great number of shear connectors are used ($S_{30}V_{2.5}$), from a practical point of view, it is suggested to use the same number of vertical struts and shear springs in the FEM ($S_{30}V_{30}$). Furthermore, there is no need to use a spacing between these smaller than the actual separation of the shear connectors.

4.1.3 Results of the FEMs

Some of the results obtained in each of the proposed FEMs are summarized in Figure 5. In this figure the FEM $S_{30}V_{30}$ (with 45 nodes and 90 beam elements) is considered under load cases Q, q and P. Figure 5 presents the axial forces throughout the axis of the concrete slab, N_c (Figure 5.A) and the shear forces per unit length at the concrete steel interface, S_{CS} (Figure 5.B). The latter parameter might be determined from the Spring Forces, F_S, or by the increment of concrete axial forces in elements between springs, ΔN_c. The calculation of S_{CS} from these parameters can be carried out taking into account the shear connector spacing, s_q, as follows:

$$S_{CS} = \frac{F_S}{s_q} = \frac{\Delta N_C}{s_q} \tag{13}$$

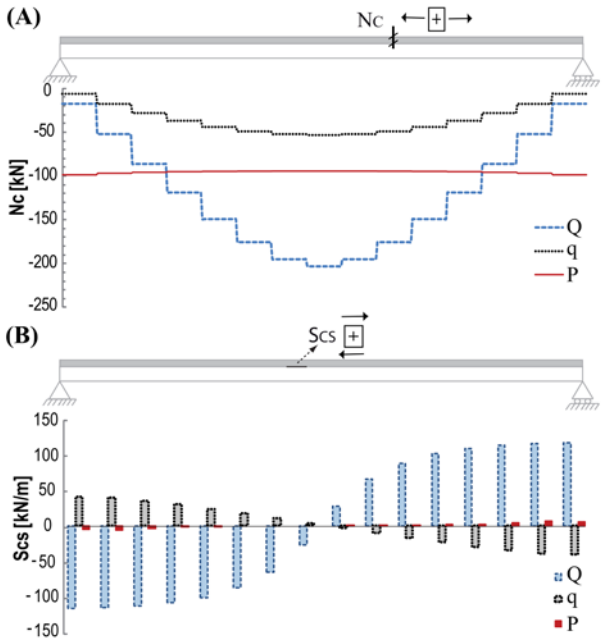

Figure 5: Axial forces in $S_{30}V_{30}$ of Example 1: (A) Concrete slab, N_c, and (B) Shear force per unit length at the concrete steel interface, S_{CS}.

As expected, the analysis of the results presented in Figure 5.A shows that compressive forces appear at the concrete slab for all loading cases. For vertical loads (such as *Q* and *q*) the maximum compressive forces are 202.88 and 53.59kN, respectively and are located at mid span, while for prestressing loads (*P*) the maximum compressive force is 100,0kN and is located at the beam edges. On the other hand, the diagrams presented in Figure 5.B illustrate the shape of the shear forces per unit length at the steel-concrete interface. The maximum values of these forces are located at the beam edges. The shear forces per unit length, S_{CS}, obtained by FEMs in different locations (x=0, 0.9 and 1.8m) in load case *Q* are presented in Table 3. The analyzed FEMs are $S_{90}V_{90}$ (number of springs lower than the actual structure) $S_{30}V_{30}$ (number of springs equal to the actual structure) and $S_{2.5}V_{2.5}$ (number of springs higher than the actual structure). Table 3 also analyzes the effects of the number of spring elements in the S_{CS}. This analysis is carried out by mean of the following percentage differences:

$$\left|\frac{S_{CS}(S_{90}V_{90}) - S_{CS}(S_{30}V_{30})}{S_{CS}(S_{30}V_{30})}\right| \quad (14)$$

$$\left|\frac{S_{CS}(S_{2.5}V_{2.5}) - S_{CS}(S_{30}V_{30})}{S_{CS}(S_{30}V_{30})}\right| \quad (15)$$

Table 3: Shear stress per unit length, S_{CS}, in Q at different locations throughout the beam length, x.

		x=0m	x=0.9m	x=1.8m
$S_{CS}(S_{90}V_{90})$	[kN/m]	114.03	106.73	57.90
$S_{CS}(S_{30}V_{30})$	[kN/m]	116.21	108.78	65.17
$S_{CS}(S_{2.5}V_{2.5})$	[kN/m]	116.48	109.16	65.50
$\left\|\frac{S_{CS}(S_{90}V_{90}) - S_{CS}(S_{30}V_{30})}{S_{CS}(S_{30}V_{30})}\right\|$	[%]	1.88%	1.88%	11.15%
$\left\|\frac{S_{CS}(S_{2.5}V_{2.5}) - S_{CS}(S_{30}V_{30})}{S_{CS}(S_{30}V_{30})}\right\|$	[%]	0.23%	0.35%	0.65%

The analysis of Table 3 shows that when a lower number of spring elements are introduced into the *FEM* ($S_{90}V_{90}$) lower values of S_{CS} are obtained. For example, at x=1.8m the value of $S_{90}V_{90}$ (57.90 kN/m) is 11.15% lower than model $S_{30}V_{30}$ (65.17 kN/m). The opposite effect appears when the number of spring elements ($S_{2.5}V_{2.5}$) is higher than that of the actual structure. Nevertheless, these differences are significantly lower in comparison with $S_{90}V_{90}$. For example, S_{CS} in $S_{90}V_{90}$ at x=1.8m (65.50 kN/m) is a 0.65% higher than model $S_{30}V_{30}$.

4.1.3- Parametric analysis of the connection stiffness K_q

The structural behavior of the composite beam is influenced, to a great extent, by the connection stiffness, K_q. Obviously, the higher this stiffness the lower the slip between concrete and steel and therefore, the more similar the behavior to that of a composite beam with full interaction. This is to say, the resistant mechanism is mainly a couple of forces, a compressive force in the slab, and a tensile force in the steel. The lower the connection stiffness, external loads are mainly balanced by two bending moments acting in the steel and concrete cross sections. To illustrate this effect Figure 6 is presented. This figure compares the values of N_{cm} and f_{cm} obtained by the model $S_{2.5}V_{2.5}$ for a stiffness K_q, [$N_{cm}(S_{2.5}V_{2.5})_{K_q}$ and $f_{cm}(S_{2.5}V_{2.5})_{K_q}$], with those values obtained for full interaction, for loading cases *Q*, q and *P* when the K_q of beam of Example 1 varies from 0 to 2.33E7kN/m^2.

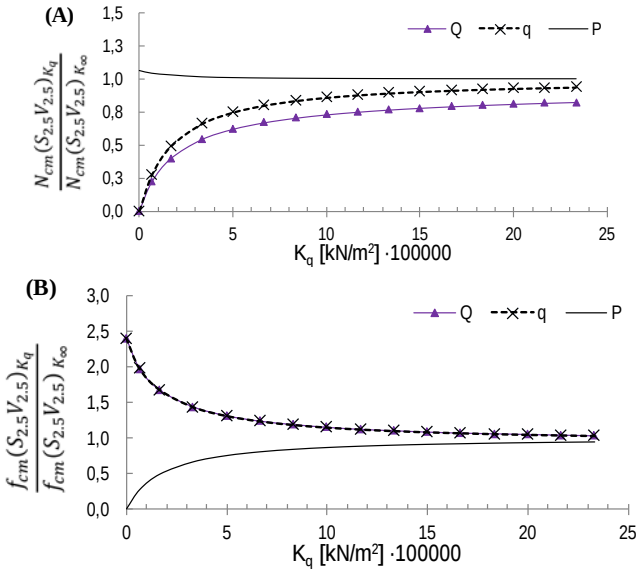

Figure 6: (A) Ratios between $N_{cm}(AE)_{K_q}$ and $N_{cm}(AE)_{K_\infty}$, and (B) Ratios between $f_{cm}(AE)_{K_q}$ and $f_{cm}(AE)_{K_\infty}$, for loading cases *Q*, *q* and *P*.

Figure 6.A shows that, obviously, the higher the K_q the more similar the values of $N_{cm}(S_{2.5}V_{2.5})_{K_q}$ and $N_{cm}(S_{2.5}V_{2.5})_{K_\infty}$, and therefore, the closer the ratio to 1. When K_q is increased this ratio tends asymptotically to 1. Figure 6.A also illustrates the important role that the flexibility of the connection plays in the structural behavior of the composite beam. In fact, in structures with flexible connections under vertical loads the error of assuming a full interaction at the concrete-steel interface cannot be neglected. For example, when K_q is fixed to 1.66E5kN/m^2 the axial forces in the model in the loading case *q* (-29.92 kN) represents 48.69% of $N_{cm}(S_{2.5}V_{2.5})_{K_\infty}$ (-61.44 kN). This difference is increased in the loading case *Q*. In this case, the $N_{cm}(S_{2.5}V_{2.5})_{K_q}$ (-107.82 kN) represents 39.48% of $N_{cm}(S_{2.5}V_{2.5})_{K_\infty}$ (-273.06 kN). On the other hand, Figure 6.B shows that the stiffness of the connection plays a significant role in all analyzed load cases. For example, when K_q is fixed to 1.66E5kN/m^2, $f_{cm}(S_{2.5}V_{2.5})_{K_q}$ (-3.49mm) represents 167.72%

of the full interaction deflection (-2.09mm). It is important to highlight that, in this particular example, this ratio is very closed to the one obtained for loading case *q* (166.98%). In loading case *P*, the influence of the connection stiffness is smaller than in the other analyzed loading cases.

The role that the connection stiffness plays in the shear force per unit length at the concrete steel interface, S_{CS}, is presented in Figure 7. This figure compares the values obtained in the model $S_{2.5}V_{2.5}$ for four different stiffnesses K_q (6.67E4, 1.67E5, 1.16E6 and 2.33E6 kN/m²) with those obtained assuming full interaction.

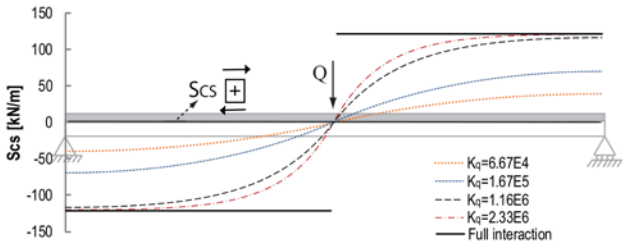

Figure 7: Shear force per unit length at the concrete steel interface, S_{CS}, in model $S_{2.5}V_{2.5}$ for different K_q in kN/m² and with a full interaction connection.

Figure 7 shows that, as expected, the higher the connection stiffness, the higher the absolute value of shear force per unit length at a given *x*, $S_{CS}(x)$. For example, the value of S_{CS} obtained for a connection stiffness of K_q=6.67E4kN/m² (-39.4kN/m) is increased to 121.38kN/m for a connection stiffness of 2.33E6kN/m² over the bearings. The higher the connection stiffness, the more similar the maximum value to the one obtained by full interaction (121.39kN/m). It is important to highlight that the maximum values for partial interaction do not exceed those obtained when full interaction is assumed. Moreover, the integral of the shear forces along the beam increases for increasing shear connection stiffness. The major differences between partial and full interaction are located at mid span as the full interaction assumption cannot predict accurately the shear force per unit length at this location.

In order to evaluate how the connection stiffness K_q influences the results of the different models, a parametric analysis is carried out in this section. In this analysis the differences of the results of model $S_{30}V_{30}$ are compared with those obtained by a model with a reduced number of spring connectors ($S_{90}V_{90}$), a model with a high number of spring connectors ($S_{2.5}V_{2.5}$) and the results of the Analytical Equation (*AE*, also referred as S_0V_0) when K_q varies from 0 to 2.33E6kN/m². Calculation of E_q of the spring connector elements (element types 4) is carried out by Equation (8).

The analysis of the effects in N_{cm} of the number of springs representing K_q is presented in Figure 8. This figure includes the percentage differences between the results of $S_{30}V_{30}$ and the Analytical Equations (also called S_0V_0), $S_{2.5}V_{2.5}$ and $S_{90}V_{90}$ for loading cases *Q* and *q*. These differences are calculated by Equation (16). The prestressing load *P* is not included because the differences with $S_{30}V_{30}$ were negligible.

$$\left|\frac{N_{cm}(S_iV_j) - N_{cm}(S_{30}V_{30})}{N_{cm}(S_{30}V_{30})}\right| \qquad (16)$$

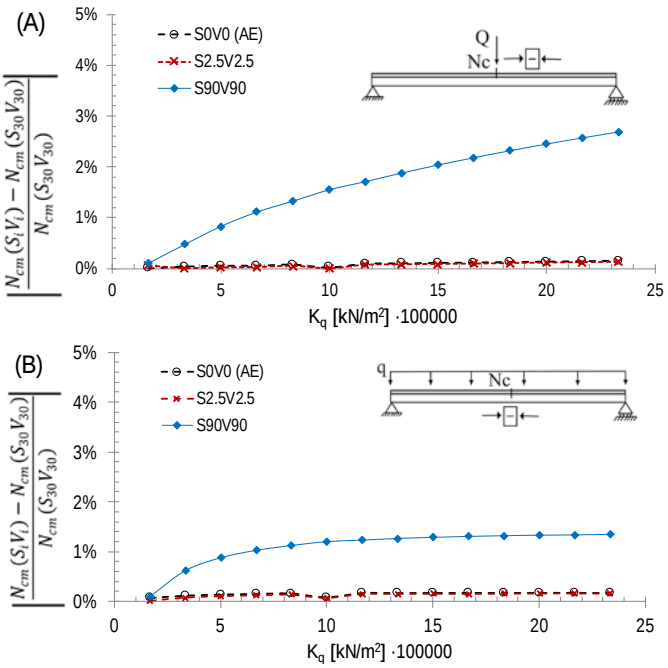

Figure 8: Percentage differences of N_{cm} between results of $S_{2.5}V_{2.5}$, $S_{90}V_{90}$ and Analytical Equations, S_0V_0 (*AE*), related to $S_{30}V_{30}$ in terms of K_q for loading cases Q (A) and q (B).

Figure 8 shows that stiffness K_q plays an important role in the results obtained by the different models. On the one hand, the differences between Analytical Equations, *AE*, and $S_{2.5}V_{2.5}$ with the $S_{30}V_{30}$ are practically negligible, as they remain lower than 0.1%. From these values, it can be concluded that similar results are obtained when a higher number of spring connectors than the actual structure is considered. Nevertheless, this is not the case in those models with lower number of springs than the actual structure (such as $S_{90}V_{90}$). In this case, the differences depend on K_q (the higher the K_q, the higher the differences). The maximum values represent a deviation of 2.69% for Q and 1.35% for q.

4.1.4- Effects of the relative height of the concrete deck and the steel beam

In order to evaluate how the steel relative height influences the results of the different models, a parametric analysis is carried out in this section. In this analysis the structure presented in Section 4.1.1 is assumed to have four different steel cross sections (IPE100, IPE300, IPE500 and IPE1000). Differences between the characteristics of these models only refer to the beam element type 2, steel beam (as each model includes the Area and Inertia of the different steel I beams). For each of the steel beams, the three following models are analyzed: model with high number of spring connectors $S_{2.5}V_{2.5}$, Analytical Equation, *AE* or S_0V_0, and model $S_{30}V_{30}$.

The axial forces at the mid span, N_{cm}, obtained in each of the models under loading cases Q and q are summarized in Table 4. This table shows that N_{cm} depends on the stiffness of the composite section. Obviously, independently of the number of spring connectors considered, the larger the I beam, the stiffer the steel beam and therefore the lower N_{cm}. For example, this is appreciable in $S_{30}V_{30}$ under loading case Q. In this structure, N_{cm} varies from -108.61kN (IPE100) to -59.69kN (IPE1000).

Table 4: Comparison of the axial forces in concrete N_{cm} for different beam types.

		IPE100		IPE300		IPE500		IPE1000	
		Q	*q*	*Q*	*q*	*Q*	*q*	*Q*	*q*
$N_{cm}(S_0V_0)$	[kN]	-110.59	-28.30	-203.07	-53.68	-137.04	-36.91	-56.95	-15.32
$N_{cm}(S_{2.5}V_{2.5})$	[kN]	-109.32	-28.12	-203.08	-53.69	-139.54	-37.34	-58.36	-15.88
$N_{cm}(S_{30}V_{30})$	[kN]	-108.61	-28.00	-203.46	-53.79	-140.54	-37.61	-59.69	-16.23
$\left\|\frac{N_{cm}(S_{2.5}V_{2.5})-N_{cm}(S_0V_0)}{N_{cm}(S_0V_0)}\right\|$	[%]	1.15%	0.64%	0.01%	0.02%	1.82%	1.16%	2.48%	3.64%
$\left\|\frac{N_{cm}(S_{30}V_{30})-N_{cm}(S_0V_{0,})}{N_{cm}(S_0V_0)}\right\|$	[%]	1.70%	1.05%	0.19%	0.21%	2.55%	1.89%	4.82%	5.97%

Table 4 also includes the percentage differences between the model with high number of spring ($S_{2.5}V_{2.5}$) connectors and the Analytical Equations, *AE* and the percentage differences between the model $S_{30}V_{30}$ and the *AE*. These differences are calculated by the following equations:

$$\left|\frac{N_{cm}(S_{2.5}V_{2.5})-N_{cm}(S_0V_0)}{N_{cm}(S_0V_0)}\right| \quad (17)$$

$$\left|\frac{N_{cm}(S_{30}V_{30})-N_{cm}(S_0V_0)}{N_{cm}(S_0V_0)}\right| \quad (18)$$

The analysis of the comparison parameters presented in Table 4 shows that the differences between $S_{2.5}V_{2.5}$ and the analytical equations depend on the I beam. In the analyzed structure, the stiffer the steel beam the larger N_{cm} obtained by $S_{2.5}V_{2.5}$. For example in the IPE1000, the percentage difference calculated by Equation (17) represents the 2.48% for *Q* and the 3.64% for *q*. The same effect is obtained when the results of $S_{30}V_{30}$ and the analytical equations are compared. In this case, the maximum differences calculated by Equation (18) represent the 4.82% for *Q* and the 5.97% for *q*.

4.2- Example 2: Three span continuous composite beam

In this section a three span continuous composite beam is analyzed. First, the main characteristics of the structure are described. Then, two parametric analyses are carried out. The first of these parametric analyses illustrates the effect of the size of the FEMs in continuous beams. The second parametric analysis shows the role of the stiffness of the connection, K_q in continuous structures with different I beams. Finally, the results obtained by the analytical equations presented by Martínez and Ortiz (1975) are compared with those obtained by different FEMs for different I beams.

4.2.1- Description of the structure

The continuous composite beam analyzed in this paragraph has three spans (3.6m+4.5m+3.6m) as presented in Figure 9.A. This beam includes the same cross section of Example 1, that is to say a concrete slab of 1m width and 0.2m thick connected to an IPE300.

As in the preceding example, the analyzed loading cases are as follows: (1) Concentrated load, *Q*, of 100kN on concrete slab at mid span, m, of the central span. (2) A uniform distributed load, *q*, of 10kN/m along the whole length of the concrete slab. (3) Two concentrated prestressing loads, *P*, of 100kN at the centroids of the edges of the concrete slab. These load cases are illustrated in Figure 9.B. The parameters analyzed for each of these loading cases are the axial force at the concrete slab at mid span, N_{cm}, and the vertical deflection at the mid span, f_m (Figure 9.C).

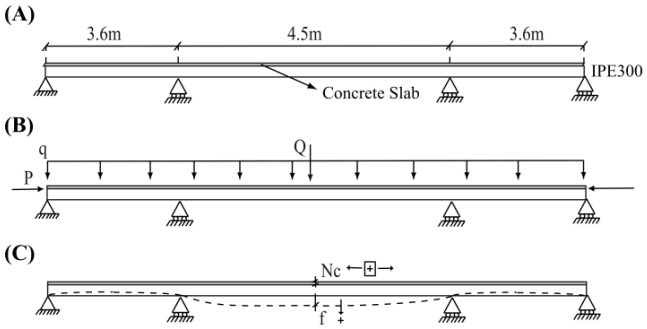

Figure 9: Example 2: (A) Geometry, (B) Analyzed load cases, (C) Analyzed parameters.

In order to analyze the effects of the element number of the *FEM*, a set of different *FEMs* have been studied. Differences between these models refer to: (1) Spacing between spring connectors. The same uniform spacing of Example 1, ($S_{2.5}$, S_5, S_{15}, S_{30} and S_{90}) is considered. (2) Spacing between vertical struts. Two different spacing ($V_{2.5}$ and V_{90}) are considered. This leads to a number of ten different FEMs that are named, as in Example 1, by mean of the combination of the two corresponding spacing (e.g. $S_{2.5}V_{90}$). The number of nodes and elements of each of the FEMs are presented in Figure 10.

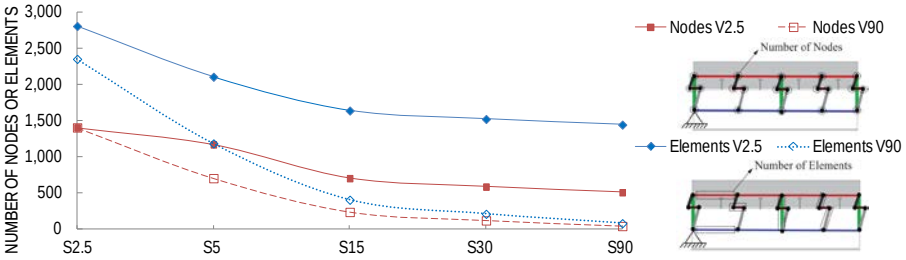

Figure 10: Number of nodes and beam elements in different FEMs of Example 2.

Figure 10 shows that in Example 2 the number of nodes ranges from 39 ($S_{90}V_{90}$) to 1404 ($S_{2.5}V_{2.5}$ and $S_{2.5}V_{90}$), while the number of beam elements ranges from 78 ($S_{90}V_{90}$) to 2808 ($S_{2.5}V_{2.5}$).

4.2.2- Results of the FEMs

A comparison of the results obtained by the analyzed FEMs is presented in Figure 11. This figure includes the percentage differences in terms of axial forces at the mid span of the concrete slab, N_{cm} (Figure 11.A) and the vertical deflection at mid span, f_m (Figure 11.B) between $S_{2.5}V_{2.5}$ (the more similar model to the Analytical Equations) and the other analyzed FEMs for loading cases *Q*, q and *P*. The comparison parameters are calculated as follows:

$$\left|\frac{N_{cm}(S_iV_j) - N_{cm}(S_{2.5}V_{2.5})}{N_{cm}(S_{2.5}V_{2.5})}\right| \quad (19)$$

$$\left|\frac{f_m(S_iV_j) - f_m(S_{2.5}V_{2.5})}{f_m(S_{2.5}V_{2.5})}\right| \quad (20)$$

The analysis of Figure 11.A shows that the differences of N_{cm} between FEMs are negligible for the loading case *P*. For vertical loads (such as *Q* and *q*) most of FEMs also present negligible differences of N_{cm} with $S_{2.5}V_{2.5}$. Nevertheless, this is not the case of those FEMs with spring connectors separated 90cm, such as $S_{90}V_{2.5}$ and $S_{90}V_{90}$. For example in $S_{90}V_{90}$, the differences of N_{cm} with $S_{2.5}V_{2.5}$ reach the 2.57% for q and 2.22% for *Q*. On the other hand, the analysis of Figure 11.B illustrates that the differences of f_m between FEMs are higher than those obtained in N_{cm}. The maximum values reach the 6.44% for *q*, the 5.91% for *Q*

and the 3.32% for *P*. These results show a slightly worse behavior than in the case of simply supported beams.

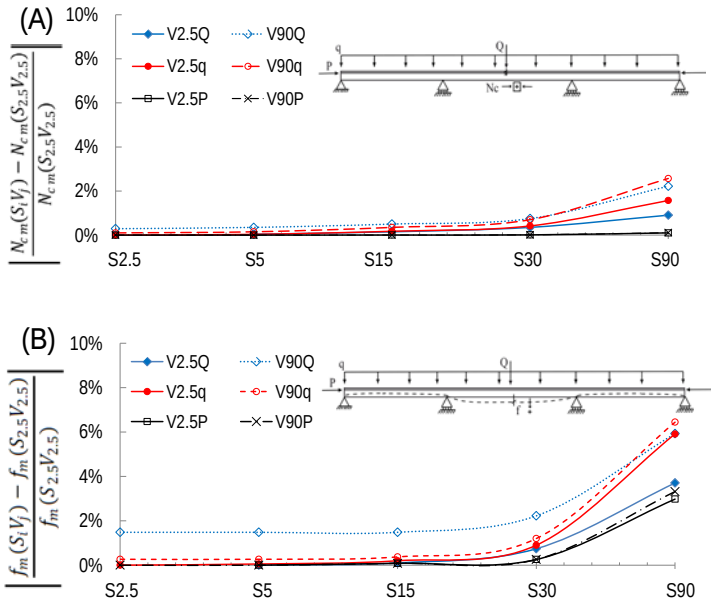

Figure 11: Comparison of the results of different FEMs with the results of $S_{2.5}V_{2.5}$ in terms of (A) N_{cm} and (B) f_m for loading cases Q, q and P. The result of each *FEM* is obtained by the intersection of the spacing S_i with the line V_j.

Some of the results obtained in each of the proposed FEMs are summarized in Figure 12 for $S_{2.5}V_{2.5}$ under loading cases Q, q and P. This figure includes the axial forces throughout the axis of the concrete slab, N_c (Figure 12.A) and the longitudinal shear forces per unit length at the steel-concrete interface, S_{CS} (Figure 12.B). The values of S_{CS} have been calculated by Equation (13).

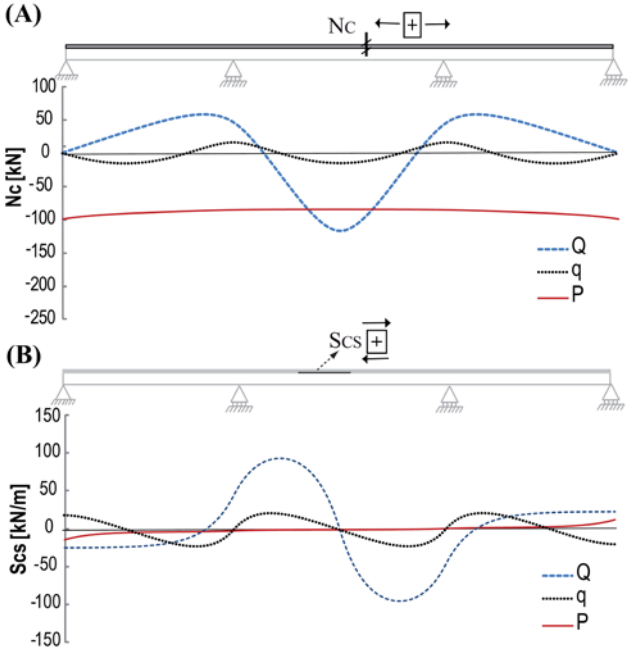

Figure 12: Internal force diagrams in Example 2 for $S_{2.5}V_{2.5}$: (A) Axial forces in concrete slab, N_c. (B) Longitudinal shear force per unit length at the concrete-steel interface, S_{CS}.

Figure 12.A shows how the axial forces, N_c, are based on the bending moment law of each loading case. In the vertical loading cases (such as *Q* and *q*) hogging bending moments appear in the inner supports. For this reason, at the proximities of these supports positive forces N_c (that is to say, tensile forces) are obtained. The maximum compressive forces for the vertical loading cases (-117.56kN in *Q* and -14.91kN in *q*) are located at mid span, *m*. On the other hand, the diagrams presented in Figure 12.B illustrate the continuous shape of the shear forces per unit length at the steel-concrete interface.

Note that as showed in Figures 3 and 4, from a practical point of view, $S_{30}V_{30}$ is the most interesting model that represents the behavior of the actual composite beam. For this reason, this model is used in all the following sections.

4.2.3- Parametric analysis of K_q for different beam sizes

In order to evaluate the effects of the connection stiffness, K_q, on statically indeterminate structures two parametric analyses are carried out in this section. In the first of these analyses N_{cm} of $S_{30}V_{30}$ is studied for stiffnesses K_q varying from 0 to 2.33E6kN/m² for loading cases *Q*, *q and P*. In this analysis, the E_q of the spring connector elements (element type 4) is calculated by Equation (8).

A comparison between N_{cm} and f_{cm} obtained by the $S_{30}V_{30}$, for a stiffness K_q, and N_{cm} and f_{cm} obtained by the same model for very stiff connections, K_∞, is presented in Figure 13.

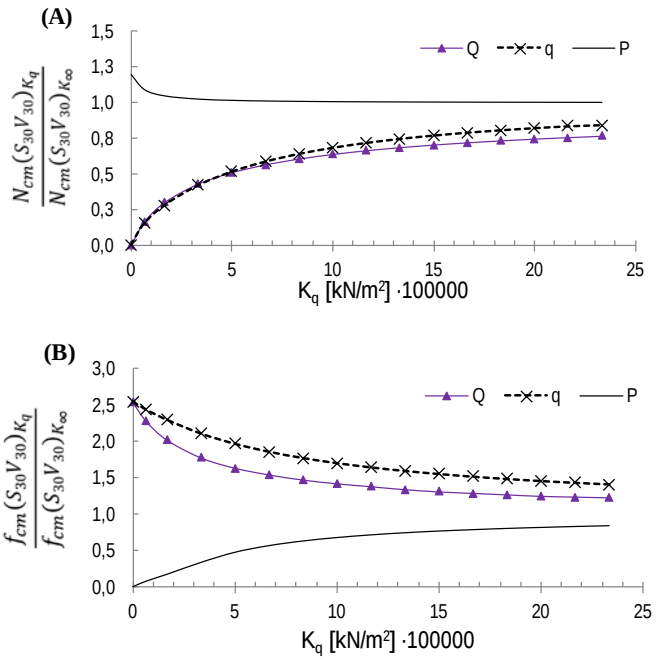

Figure 13: (A) Ratio between $N_{cm}(S_{30}V_{30})_{K_q}$ and $N_{cm}(S_{30}V_{30})_{K_\infty}$, and (B) Ratios between $f_{cm}(S_{30}V_{30})_{K_q}$ and $f_{cm}(S_{30}V_{30})_{K_\infty}$, for loading cases *Q*, *q* and *P*.

Figure 13.A shows that, as expected, the higher the K_q the more similar the values of $N_{cm}(S_{30}V_{30})_{K_q}$ and $N_{cm}(S_{30}V_{30})_{K_\infty}$, and therefore, the closer the ratio to 1. This figure also illustrates that the flexibility of the connection plays an important role in the structural behavior of continuous composite beams. In fact, in structures with partial interaction under vertical loads differences with full interaction might be significant. For example, when K_q is1.67E5kN/m² the axial force in the model in the loading case *Q* (-53.53 kN) represents the 29.90% of $N_{cm}(S_{30}V_{30})_{K_\infty}$ (-179.03 kN). On the other hand, the analysis of the deflections presented in Figure 13.B shows that the lesser the connection stiffness, the higher the differences

between ratios. For example, when K_q is 1.67E5kN/m^2 the vertical deflection in the loading case Q (-1.98mm) represents the 201.38% of the deflection for full interaction (-0.98mm). So, service limit state should be carefully checked with adequate models.

Figure 14 presents a comparison between the shear forces per unit length at the concrete steel interface, S_{CS}, in model $S_{30}V_{30}$ with five connection stiffnesses K_q. This figure shows that the stiffer the connection the closer the maximum values of S_{CS} to those obtained for full interaction. As in the case of the simply supported beam presented in Figure 7, the maximum values of the full interaction are not exceeded by the models with partial interaction. In addition, it is important to highlight that major differences appear between the results obtained by the partial and the full interaction at the proximities of the inner supports and mid span. Because of these differences, the integral of the shear forces throughout the beam obtained by the models with partial interaction are lower than those obtained by the model with full interaction.

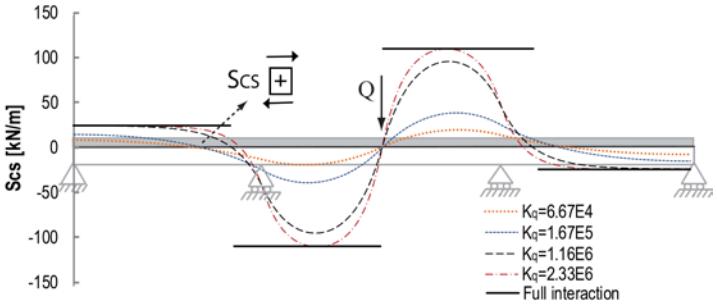

Figure 14: Shear force per unit length at the concrete steel interface, S_{CS}, in model $S_{30}V_{30}$ for different K_q (in kN/m^2) and with a full interaction.

The second parametric analysis presented in this section studies how the connection stiffness K_q influences the behavior of the model $S_{30}V_{30}$ with different I beams. In this analysis the structure presented in Section 4.2.1 is assumed to have four different beams (IPE100, IPE300, IPE500 and IPE1000). The characteristics of the models of these structures only differ in the Area and Inertia of the steel beam element (element type 2). This parametric analysis is focused on the bending moments at mid span, M_m. The values of these bending moments can be determined either from the internal forces (axial forces and bending moments acting on the concrete slab and the steel beam) or the external forces (external reactions on the boundary conditions). In this paper, the latter method has been used. This is to say, the bending moment at cross section m at mid span has been calculated by equilibrium equations from the reactions obtained in the finite element model.

The effect of the stiffness connection in different I beams in the loading case Q is summarized in Figure 15 according to the following ratio:

$$1 - \left| \frac{R_i(S_{30}V_{30})_{K_q}}{R_i} \right| \text{ , i=1 for the outer supports and i=2 for inner supports} \quad (21)$$

in which $R_i(S_{30}V_{30})_{K_q}$ represents the vertical reactions obtained for an stiffness K_q, and R_i represents the vertical reactions for the continuous beam. The subindex i refers to the location of the support (i=1 for the outer supports and i=2 for the inner ones). Obviously, the closer the ratio of Equation (21) to 0, the more similar the reactions obtained by the models with flexible connection, $R_i(S_{30}V_{30})_{K_q}$ to those of the continuous beam. The maximum ratios of each I beam are also indicated in Figure 15.

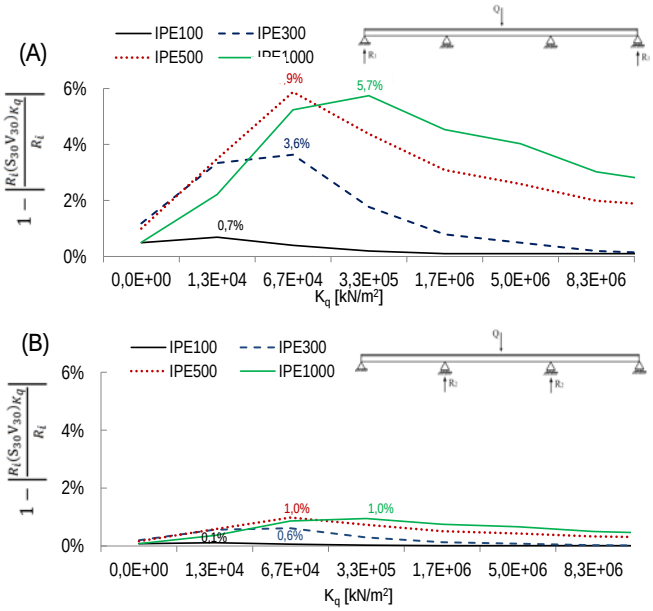

Figure 15: Ratio presented in Equation (21) in terms of K_q for a $S_{30}V_{30}$ with different I beams (IPE100, IPE300, IPE500 and IPE1000) under loading case *Q*. Reaction at the outer supports R_1, (A), and at the inner supports R_2, (B).

With $M_m(S_{30}V_{30})_{K_q}$ being the bending moment at mid span obtained for an stiffness K_q, and $M_m(S_{30}V_{30})_{K_\infty}$ being the bending moment at mid span obtained for a very high stiffness, K_∞, the following ratio can be defined to present the changes of the bending moments produced by the shear connector stiffness:

$$1 - \left| \frac{M_m(S_{30}V_{30})_{K_q}}{M_m(S_{30}V_{30})_{K_\infty}} \right| \tag{22}$$

Figure 16 summarizes the differences between $M_m(S_{30}V_{30})_{K_q}$ and $M_m(S_{30}V_{30})_{K_\infty}$ for loading cases Q and q. This figure shows that the ratio in Equation 22, depends on the stiffness, K_q, the I beam and the loading case. The analysis of loading case *Q* (Figure 16.A) shows that the bending moments for null K_q correspond with those obtained by K_∞, and therefore, null ratios are obtained. For intermediate K_q a maximum ratio is obtained for each I beam. The maximum ratios obtained in loading case *Q* (0.33% for the IPE100, 1.76% for the IPE300, 3.47% for the IPE500 and 2.67% for the IPE1000) are found in a range of K_q between 6.67E4kN/m² (IPE100) and 1.67E6kN/m² (IPE10000). Because of the statically redundancy of the structure, the location of this maximum is not easy to predict. Furthermore, the depth, the area and the inertia of the I beam are related with two different resistant mechanisms (the pair of forces between the concrete and the steel and the flexural mechanism). The resistant mechanism of the pair of axial forces between the concrete and the steel section depends on the depth and the area of the I beam. In this way, the higher the depth or the area of the IPE section, the higher the axial forces in both concrete and steel. On the other hand, the flexural stiffness of the I beam, depends on the IPE inertia. Obviously, the higher the inertia the higher the flexural behavior of the steel beam and therefore, the lower the axial force in the concrete. The effects of the stiffness K_q in loading case q (Figure 16.B) are significantly lower. In fact, the maximum ratios obtained (0.71% for the IPE1000) can be considered negligible as they do not reach the 1%.

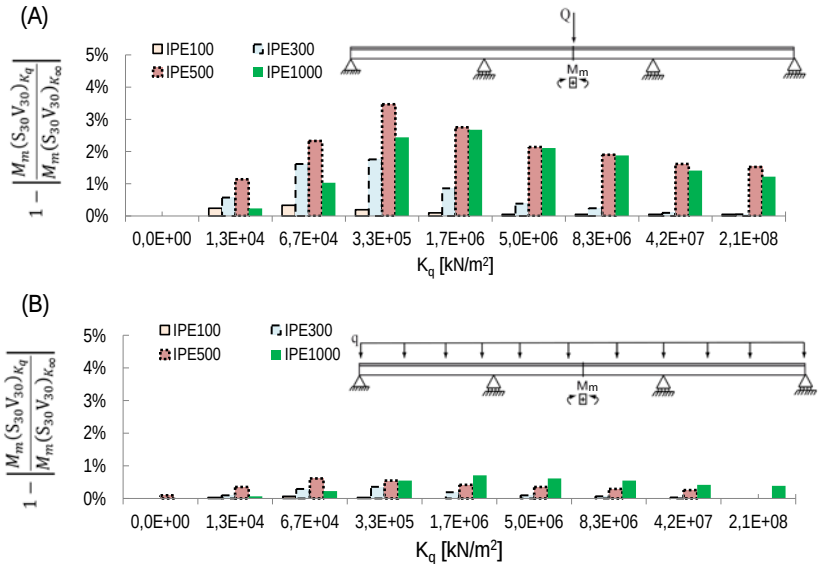

Figure 16: Ratio presented in Equation (21) in terms of K_q for a $S_{30}V_{30}$ with different I beams (IPE100, IPE300, IPE500 and IPE1000) under loading case *Q* (A), and *q* (B).

4.2.4- Comparison with the Analytical Equations

In this section the results of the Analytical Equations, presented by Martínez and Ortiz (1975) are compared with those obtained by two FEMs. These FEMs correspond with a model with practically continuous steel-concrete connection, $S_{2.5}V_{2.5}$, and a model $S_{30}V_{30}$. The first step to carry out this comparison consists on extending the analytical equations to deal with continuous structures, as in the literature they are only proposed to simply supported structures. To do so, the continuous beam can be replaced by an equivalent simply supported beam for each loading case. In this way, the bending moments at mid span can be obtained by equilibrium equations. It is to highlight to apply equilibrium equations using Martinez and Ortiz formulas, the support reactions have to be calculated first with the model presented in this paper (in this section the model $S_{30}V_{30}$ has been used). The possibility of using the reactions for a continuous beam given by the strength of materials theory is always there, but some error will be introduced in the solution.

The N_{cm} value obtained by the analytical equations (S_0V_0), $S_{2.5}V_{2.5}$ and $S_{30}V_{30}$ for different I beams (IPE100, IPE300, IPE500 and IPE1000) with K_q of 1.13E6kN/m² in loading cases *Q* and *q* are presented in Table 5. This table shows that for light I beams (such as the IPE100) the analytical equations provides higher values than the *FEMs*. The opposite effect is produced in stiff I beams (such as IPE500 and IPE1000). Table 5 also presents a comparison between the results obtained by the different models. This comparison is carried out by mean of the absolute value of the ratios presented in Equations (17) and (23).

Table 6: Comparison of the axial forces N_{cm} for different steel I beams.

		IPE100		IPE300		IPE500		IPE1000	
		Q	*q*	*Q*	*q*	*Q*	*q*	*Q*	*q*
$N_{cm}(S_0V_0)$	[kN]	-67.25	-8.86	-117.64	-14.83	-77.64	-9.89	-30.34	-3.96
$N_{cm}(S_{2.5}V_{2.5})$	[kN]	-65.94	-8.85	-117.63	-14.91	-80.29	-10.48	-32.19	-4.23
$N_{cm}(S_{30}V_{30})$	[kN]	-65.90	-8.85	-117.56	-14.88	-80.40	-10.47	-32.28	-4.22
$\left\|\frac{N_{cm}(S_{2.5}V_{2.5})-N_{cm}(S_0V_0)}{N_{cm}(S_0V_0)}\right\|$	[%]	1.95%	0.17%	0.01%	0.55%	3.42%	5.93%	6.07%	6.58%
$\left\|\frac{N_{cm}(S_{30}V_{30})-N_{cm}(S_{2.5}V_{2.5})}{N_{cm}(S_{2.5}V_{2.5})}\right\|$	[%]	0.05%	0.00%	0.06%	0.18%	0.14%	0.06%	0.29%	0.01%

$$\left|\frac{N_{cm}(S_{30}V_{30}) - N_{cm}(S_{2.5}V_{2.5})}{N_{cm}(S_{2.5}V_{2.5})}\right| \quad (23)$$

The analysis of the ratios presented in Table 5 shows that the differences between the results of the Analytical Equations (S_0V_0) and $S_{2.5}V_{2.5}$ depend on the I beam. The stiffer the steel beam the larger the differences. The maximum values (6.07% for *Q* and 6.58% for *q*) are obtained for the IPE1000. These differences can be explained by the role that the stiffness of the steel beam plays in the overall behavior of the continuous composite beams (and therefore, on their reactions). On the other hand, the second ratio presented in Table 5 illustrates that in this particular case, the differences between $S_{2.5}V_{2.5}$ and $S_{30}V_{30}$ are negligible.

5- Conclusions

In addition to their computational cost, the use of analytical equations to analyze composite beams with partial interaction is limited in practice. In fact, this procedure is not always applicable to a number of common structures (such as statically indeterminate and tapered beams, non-continuous shear connector distributions or complex load cases). To fill these gaps, a two dimensional Finite Element Model (*FEM*) is proposed in this paper to simulate the behavior of composite beams with partial interaction. This model includes the following six different types of frame elements: the concrete slab, the steel beam, the spring connectors to simulate the concrete-steel interface, and two kind of vertical struts to simulate de distance between concrete and steel sections' centroid and the steel-concrete interface. Compared with the analytical equations presented in the literature, this method presents the following advantages: (1) Intuitiveness, as the different elements of the model present a close and easy to understand relation with the structural behavior of the composite beam. (2) Applicability, as the method directly provides useful information for the design work. In fact, the application of this method include any beam geometry, any distribution of non-uniform shear connectors and any applied load for both determinate and indeterminate beams. (3) Versatility and generalization in dealing with any combination of loading and boundary conditions. Furthermore, the proposed model does not require assuming a continuous connection at the concrete-steel interface. (4) Easy elaboration of models. (5) Possible widespread use of the model, as it can be implemented in any structural software. The presented method is able to simulate the shear deformability. Nevertheless, in the current work, shear deformability was not considered because the results were compared and validated with the analytical equations, which do not include this deformation. The effects of the shear deformability will be addressed in detail in a future research

To evaluate the simulation of the proposed methodology, two examples (a simply supported beam and a continuous beam) have been analyzed according to different load cases. In each of these structures different parametric analysis have been carried out and the results were compared with those obtained by the analytical equations presented in the literature. The analysis of these structures leads to the following conclusions: (1) The FEMs with reduced spacing among spring connectors reproduce correctly the results of the analytical equations. Note that the analytical equations might be regarded as the exact solution. This is misleading, as the physical behavior of the discrete behavior of the shear connectors might be best modeled by the proposed FEM. This model includes a spring element at the steel-concrete interface, there where the shear connectors are present. Even though the most accurate simulation of the physical behavior is achieved when a great number of vertical shear connectors are used, from a practical point of view, it is suggested to use the same number of vertical struts and shear springs in this FEM. (2) As expected, the stiffness of the concrete and steel connection influences the behavior of the composite beams. In statically determined beams, the higher the stiffness of the connection the larger the differences between the analytical equations and the FEMs are. This effect is more significant in those structures with higher spacing of spring elements. On the other hand, in the case of continuous beams the maximum differences with the analytical equations depend on the depth of the I beam. In fact, the maximum

differences are obtained for intermediate shear stiffnesses. Because of the statically redundancy of the structure, the location of this maximum cannot be easily predicted. Furthermore, the depth, the area and the inertia of the I beam are related with two different resistant mechanisms (the pair of forces between the concrete and the steel and the flexural mechanism).In the prestressing of the concrete slab the effects of the stiffness of the connection can be neglected. (3) As expected, the models show how the values of shear forces per unit length obtained by models with partial interaction do not exceed those values obtained when full interaction is assumed. The integral of shear forces throughout the beam is lower in those models with partial interaction than in models with full interaction. (4) The proposed model has validated the use of the analytical equations to approximate the behavior of continuous beams. Albeit reasonable, until now, this conclusion was untested as in the literature these equations were only presented to deal with simply supported beams. The presented method will be developed in the future to address tapered beams, the effect of shear deformation, 3D structures and nonlinear behavior of concrete slab, steel beam and shear connectors.

Acknowledgements:

Part of this work was done through a collaborative agreement between Tongji University (China) and Technical University of Catalonia, UPC, BarcelonaTech. This included an exchange of faculty financed by the Chinese government. The financial support from the High End Foreign Experts program from the Chinese government is greatly appreciated.

References:

1. Al-deen, S., Ranzi, G. and Vrcelj, Z. (2011) Shrinkage effects on the flexural stiffness of composite beams with solid concrete slabs: An experimental study, *Engineering Structures,* 33(4), 1302-1315.
2. Martínez, J. and Ortiz, J. (1975) Composite Construction, *Construcción Mixta*, Editorial Rueda (In Spanish).
3. Degtyarev, V. V. (2014) Strength of composite slabs with end anchorages. Part I: Analytical model, *Journal of Constructional Steel Research 94*, 150-162.
4. Dall'Asta A, Zona A. (2002) Non-linear analysis of composite beams by a displacement approach. *Computers and Structures;* 80(27–30), 2217–28.
5. Danku, G. Dubina, D. and Ciutina A. (2013b) Influence of steel-concrete interaction in dissipative zones of frames: I - Experimental study, *Steel and Composite Structures*, 15(3), 299-322
6. Danku, G. Dubina, D. and Ciutina A. (2013b) Influence of steel-concrete interaction in dissipative zones of frames: II - Numerical study, *Steel and Composite Structures*, 15(3), 323-342.
7. Daniels BJ, Crisinel M. (1993) Composite slab behavior and strength analysis. Part 1: calculation procedure. *ASCE Journal of Structural Engineering*, 119(1):16–35.
8. EN 1994-1-1: (1994a) Eurocode 4 - Design of composite steel and concrete structures - Part 1: General rules and rules for buildings, European Committee of Normalization.
9. EN 1994-2: (1994b) Eurocode 4 - Design of composite steel and concrete structures - Part 2: General rules and rules for bridges, European Committee of Normalization.
10. Guezouli, S. Lachal, A. (2012) Numerical analysis of frictional contact effects in push-out tests, Engineering Structures, 40, 39-50.
11. Hsu, C.T., Punurai, S., Punurai, W. Magdi, Y. (2014) New composite beams having cold-formed steel joists and concrete slab, *Engineering Structures*, 71(15), 187-200.
12. Huang, Y., Yi, W. Zhang, R. and Xu, M. (2014) Behavior and design modification of RBS moment connections with composite beams*, Engineering Structures*, 59, 39-48.

13. Kim, S.H., Choi, J., Park, S.J., Ahn, J.H., Jung, C.Y. (2014) Behavior of composite girder with Y-type perfobond rib shear connectors, *Journal of Constructional Steel Research*, 103, 275-289.
14. Limoeiro de Oliveira, T.J. Batista, E. (2009) Modelling beam-to-girder semi-rigid composite connection with angles including the effects of concrete tension stiffness, *Engineering Structures*, 31, 1865-1879.
15. Martinelli, E., Nguyen, Q.H., Hjiaj, M. (2012) Dimensionless formulation and comparative study of analytical models for composite beams in partial interaction, *Journal of Constructional Steel Research*, 75, 21-31.
16. Mirza, O., Uy, B. (2010) Effects of the combination of axial and shear loading on the behaviour of headed stud steel anchors, *Engineering Structures*, 32(1), 93-105.
17. Newmark NM, Siess CP, Viest IM. Tests and analysis of composite beams with incomplete interaction. *Proc Soc Exp Stress Anal* 1951; 9(1):7592.
18. Nie, J. Fan, J. Caib, C.S. (2008) Experimental study of partially shear-connected composite beams with profiled sheeting, *Engineering Structures*, 30, 1-12.
19. Park, Y.H., Kim, S.H., Lee, S.L. Choi, J.H. (2013) Approximate analysis method for composite beams with partial shear interaction using Fourier Series. *International Journal of Steel Structures*, 13(2), 219-227.
20. Prakash, A., Anandavalli N., Madheswaran C. K., Rajasankar J. and Lakshmanan N. (2011) Three Dimensional FE Model of Stud Connected Steel-Concrete Composite Girders Subjected to Monotonic Loading, *International Journal of Mechanics and Applications*, 1(1): 1-11.
21. Proco G, Spadea G, Zinno R. (1994) Finite element analysis and parametric study of steel–concrete composite beams. *Cement and Concrete Composites*; 16: 261–72.
22. Queiroz, F.D., Vellasco, P.C.G.S, Nethercot, D.A. (2007) Finite Element modeling of composite beams with full and partial shear connection, *Journal of Constructional Steel Research*, 63(4), 505-521.
23. Queiroz, F.D., Queiroz, G. and Nethercot, D.A. (2009) Two-dimensional FE model for evaluation of composite beams, I: Formulation and Validation, *Journal of Constructional Steel Research*, 65, 1055-1062.
24. Queiroz, F.D., Queiroz, G. and Nethercot, D.A. (2009) Two-dimensional FE model for evaluation of composite beams, II: Parametric Study, *Journal of Constructional Steel Research*, 65, 1063-1074.
25. Ranzi, G. Bradford, M.A. (2007) Composite beams with both longitudinal and transverse partial interaction subjected to elevated temperatures, *Engineering Structures*, 29, 2737-2750.
26. Sakr, M.A, Sakla, S.S.S. (2009) Long-term deflection of cracked composite beams with nonlinear partial shear interaction - A study using neural networks, *Engineering Structures*, 31(12), 2988-2997.
27. Salari MR, Spacone E, Shing PB, Frangopol DM. (1997) Non-linear analysis of composite beams with deformable shear connectors. *ASCE Journal of Structural Engineering*; 124(10):1148–54.
28. Soty, R., Shima, H. (2013) Formulation for shear force-relative displacement relationship of L-shape shear connector in steel-concrete composite structures, *Engineering Structures*, 46, 581-592.
29. Sousa, J.B., Oliveira, C.E.M. and Silva, A. (2010) Displacement-based nonlinear finite element analysis of composite beam-columns with partial interaction, *Journal of Constructional Steel Research*, 66, 772-779.
30. Szabó, B. (2006) Influence of Shear Connectors on the elastic behavior of composite girders. Phd Thesis. Helsinki University of Technology Publications in Bridge Engineering.

31. Tahmasebinia, F., Ranzi, G. and Zona, A. (2013) Probabilistic three-dimensional finite element study on composite beams with steel trapezoidal decking, *Journal of Constructional Steel Research*, 80, 394-411.
32. Titoum, M., Tehami, M., Achour, B. and Jaspart, J.P. (2008) Analysis of Semi-Continuous Composite Beams with Partial Shear Connection Using 2-D Finite Element Approach, *Asian Journal of Applied Sciences*, 1(3), 185-205.
33. Turmo, J. and Mirambell, E. (2002), Calculation model for composite structures with imperfect interaction. Modelo de cálculo para estructuras mixtas con interacción imperfecta*, II International conference of ACHE (Asociación Científico Técnica del Hormigón Estructural), 11-14 November, Madrid.* (In Spanish).
34. Wang, AJ Chung, KF (2006) Integrated analysis and design of composite beams with flexible shear connectors under sagging and hogging moments, *Steel and Composite Structures*, 6, 459-477.
35. Zona, A. and Ranzi, G. (2014) Shear connection slip demand in composite steel-concrete beams with solid slabs, *Journal of Constructional Steel Research*, 102, 266-281.